

Protective effects of the notoginsenoside RI on acute lung injury by regulating the miR-128-2-5p/Tollip signaling pathway in rats with severe acute pancreatitis

Innate Immunity
2022, Vol. 28(1): 19–36
© The Author(s) 2022
Article reuse guidelines:
sagepub.com/journals-permissions
DOI: 10.1177/17534259211068744
journals.sagepub.com/home/ini
SAGE

Ju He^{1,*}, Ming-wei Liu^{2,*}, Zhi-yi Wang¹ and Rong-jie Shi³ 

Abstract

Notoginsenoside RI (NG-RI), the extract and the main ingredient of *Panax notoginseng*, has anti-inflammatory effects and can be used in treating acute lung injury (ALI). In this study, we explored the pulmonary protective effect and the underlying mechanism of the NG-RI on rats with ALI induced by severe acute pancreatitis (SAP). miR-128-2-5p, ERK1, Tollip, HMGB1, TLR4, I κ B, and NF- κ B mRNA expression levels were measured using real-time qPCR, and TLR4, Tollip, HMGB1, IRAK1, MyD88, ERK1, NF- κ B65, and p-I κ B- α protein expression levels using Western blot. The NF- κ B and the TLR4 activities were determined using immunohistochemistry, and TNF- α , IL-6, IL-1 β , and ICAM-1 levels in the bronchoalveolar lavage fluid (BALF) using ELISA. Lung histopathological changes were observed in each group. NG-RI treatment reduced miR-128-2-5p expression in the lung tissue, increased Tollip expression, inhibited HMGB1, TLR4, TRAF6, IRAK1, MyD88, NF- κ B65, and p-I κ B- α expression levels, suppressed NF- κ B65 and the TLR4 expression levels, reduced MPO activity, reduced TNF- α , IL-1 β , IL-6, and ICAM-1 levels in BALF, and alleviated SAP-induced ALI. NG-RI can attenuate SAP-induced ALI. The mechanism of action may be due to a decreased expression of miR-128-2-5p, increased activity of the Tollip signaling pathway, decreased activity of HMGB1/TLR4 and ERK1 signaling pathways, and decreased inflammatory response to SAP-induced ALI. Tollip was the regulatory target of miR-128-2-5p.

Keywords

Notoginsenoside RI, pancreatitis, acute lung injury, miR-128-2-5p, Toll interacting protein, rats

Date received: 15 July 2021; revised: 14 November 2021; accepted: 7 December 2021

Introduction

In acute pancreatitis, especially severe acute pancreatitis (SAP), the pancreatic cell injury is caused by abnormally activated pancreatic enzymes, activated monocyte macrophages, and a triggered cascade effect of pro-inflammatory cytokine synthesis and release.¹ The systemic inflammatory response syndrome occurs due to the aggravation of the pancreatic injury, resulting in injury, insufficiency, and even failure of the distal viscera. Acute lung injury (ALI) is one of the most common and severe complications of SAP.² The acute pancreatitis-associated lung injury is the leading cause of early high mortality in SAP. Among SAP-related systemic complications, lung complications are the most severe and common. Hypoxemia and acute respiratory distress syndrome (ARDS) are experienced by 30%–50% of patients with SAP.^{1,3,4} Pulmonary lesions and functional changes often occur earlier in SAP than in organs (such as the heart, liver, and kidney) and are closely associated with early mortality in SAP. Thus, mortality reaches 60% in

patients with SAP and pulmonary complications, such as ALI and ARDS. Mortality reaches more than 65% in patients with SAP due to ARDS, and specific treatments for patients with SAP and ALI are not available.⁵

Panax notoginseng, one of the most valuable traditional Chinese medicine (TCM), is obtained from the roots and the rhizomes of *P. notoginseng* (Burkill) F.H. Chen. P.

¹Department of Gastrointestinal Surgery, First Affiliated Hospital of Dali University, Dali City, China

²Department of Emergency, The First Hospital Affiliated of Kunming Medical University, Kunming, China

³Department of Gastroenterology, First Affiliated Hospital of Dali University, Dali City, China

*Contributed equally.

Corresponding author:

Rong-jie Shi, Department of Gastroenterology, First Affiliated Hospital of Dali University, 32 Carlsbury Avenue, Dali City 671000, China.
Email: 3168167636@qq.com



notoginseng saponins (PNS) are highly purified isolates extracted from *P. notoginseng* plants.⁶ These saponins possess pharmacological effects, such as dilation of blood vessels, improvement of microcirculation, anti-inflammation, protection of tissue antioxidation, inhibition of lipid peroxidation, reduction of Ca²⁺ influx, and influence on free-radical production.⁷ PNS protect against damage from myocardial ischemia/reperfusion by inhibiting the activation of NF- κ B and decreasing the expression of the intercellular adhesion molecule-1 (ICAM-1) in neutrophils.^{8,9} Yan et al.¹⁰ have found that the neuroprotective effect of PNS may be based on the direct inhibition of the macrophage TLR pathway. PNS consist of five saponin monomers, namely, R1, Rb1, Rg1, Re, and Rd. The notoginsenoside R1 (NG-R1), the main active ingredient of PNS, inhibits the activation of NF- κ B and decreases the production of inflammatory mediators, such as TNF- α , IL-1 β , and ICAM-1,¹¹ however the specific mechanism remains unclear.

The Toll-acting protein (Tollip), a linker protein, is first discovered by Burns et al.¹² Tollip, which is composed of 274 amino acids, is a small protein containing three regions, namely, C2, C-end CUE, and N-end Tom1-binding domain (TBD) areas. The main function of the C2 domain contained in the central region is to transport the Tollip to specific nuclear endosomes. CUE at the C-terminus plays an important role in the interaction of ubiquitinated proteins, whereas the N-terminus contains a TBD, which participates in the interaction of Tom1, a protein that can bind to ubiquitin.¹³ Tollip participates in the immune response of the signaling pathway of TLRs.¹⁴ TLRs are expressed in macrophages and other white blood cells, and represent PRR molecules. TLRs recognize inflammatory factors, activate intracellular signaling pathways, stimulate pathogen-associated and injury-related molecular patterns,¹⁵ and activate two classic transduction pathways, including the MyD88-dependent conduction pathways. The MyD88-dependent conduction pathways eventually activate the NF- κ B conduction pathway,¹⁶ further regulating the inflammatory response induced by various causes. Tollip can reduce the transcriptional activity of NF- κ B by down-regulating the related MyD88-dependent TLR signaling pathway, thereby inhibiting the activation of inflammatory cells and reducing the inflammatory response.¹⁴ Therefore, Tollip plays an important role in the negative regulation of the inflammatory response.

MicroRNA (miR), a noncoding RNA that has a length of 20–22 bp, is involved in the regulation of multiple cellular processes, such as cell proliferation, differentiation, aging, apoptosis, metabolism, inflammation and immune response, organogenesis, and tumor formation.¹⁷ miRs are complementary to the 3'-end noncoding region of their target mRNAs. As such, any target mRNA molecule is inhibited at the translation level or degraded.¹⁸ Conversely, miRs can function as an unconventional mediator for transcriptional gene activation through chromatin remodeling at enhancer regions and

activate gene expression.¹⁸ miRs regulate inflammation. For instance, the high expression levels of miR-146a, miR-155, and miR-181b evidently inhibit LPS-induced TNF- α , IL-6, and IL-1 β released from the lung tissue of rats, thereby inhibiting lung inflammation.¹⁹ miR-124 mediates the inflammatory pathogenesis of Parkinson's disease.²⁰ miR-548a-3p regulates the inflammatory response of rheumatoid arthritis (RA) by regulating the activity of the TLR4/NF- κ B signaling pathway.²¹ miR-10a-5p regulates joint inflammation in synoviocytes,²² however the specific mechanism remains unclear and needs further study.

miR-128, which is abnormally expressed in various tumors, is widely involved in various processes of tumor biology.²³ A decrease in the miR-128 expression reduces the NF- κ B activity and the inflammatory damage to nerve cells by targeting the PPAR- γ modulation.²⁴ miR-128-2-5p expression in patients with RA is remarkably higher than that in the control,²⁵ which suggests that the miR-128-2-5p is involved in RA-induced inflammation.

However, whether miR-128-2-5p mediates the regulatory mechanism of ALI remains unclear. Previous research found that Tollip can negatively regulate the activities of HMGB1/TLR4 and ERK/NF- κ B pro-inflammatory pathways and reduce the inflammatory response,²⁶ and that miR-128-2-5p can regulate inflammation through pro-inflammatory pathways, such as NF- κ B in sepsis-induced lung tissue.²⁷ In this study, we predicted that miR-128-2-5p is a possible target of Tollip for regulation through the TargetScan. Therefore, we hypothesized that miR-128-2-5p is involved in the development of ALI induced by SAP. We further determined whether NG-R1 can regulate Tollip through the miR-128-2-5p, inhibit the HMGB1/TLR4 and the ERK/NF- κ B pro-inflammatory pathways, reduce lung inflammation, and alleviate ALI induced by SAP. Results provided a new rationale for the use of the NG-R1 in the treatment of inflammation-related ALI. For these studies, we selected the known model of pancreatitis based on inflammatory lung injury induced by hyperstimulation that most closely resembled clinical ALI associated with severe pancreatitis.

Material and methods

Preparation of NG-R1

NG-R1 (C₄₇H₈₀O₁₈, molecular mass = 933.16, 99.0% purity) was purchased from Jiangsu Yongjian Pharmaceutical Technology Co., Ltd (Jiangsu, China). It was dissolved in sterile water to obtain 1 mM stock solution, which was stored at 20°C.

Cell culture

RAW264.7 macrophages (Heilongjiang Cancer Institute, Harbin, China) were grown in DMEM supplemented with

5% FBS, 100 U/ml penicillin, 100 U/ml streptomycin, and 50 µg/l amphotericin B. RAW264.7 macrophages' culture conditions were maintained at 37°C in a humidified atmosphere of air and 5% CO₂, and cells were subcultured into 6-well plates and maintained until subconfluence was achieved. NG-R1 was prepared at different concentrations (10, 20, 30, 40, and 50 µM) in accordance with a previous report.¹¹ RAW264.7 macrophages were pre-incubated with NG-R1 for 24 h and stimulated using LPS (1 g/l).

Mir mimics, inhibitor, and gene transfection

RAW264.7 macrophages were cultured in 6-well plates until 40% confluence was achieved. miR-128-2-5p mimics, miR-128-2-5p mimic-negative control (NC), miR-128-2-5p inhibitor, and miR-128-2-5p inhibitor-NC were mixed with Lipofectamine 2000 (Invitrogen), and the mixture was added to the cell culture medium in accordance with the manufacturer's instructions. The cultures were transfected for 24 h, and the total RNA and protein were extracted from the cells and subjected to real-time PCR (RT-PCR) and Western blot, respectively. The miR-128-2-5p mimics, inhibitor, and NC oligonucleotides were purchased from Sangon Biological Engineering Co., Ltd (Shanghai, China). The transfection efficiency was determined using qRT-PCR.

Detection of the cell viability by using the CCK-8 assay

RAW264.7 macrophages transfected with recombinant plasmids or treated with NG-R1 for 24 h in accordance with the experimental requirements were seeded into 96-well plates at a density of 5×10^3 cells/well, added with 20 µl CCK-8 solution (5 g/l), and cultured at 37°C for 1 h. Then, the culture was terminated. The blank hole was set to zero. The OD value of each hole was detected at 450 nm after 3 min of oscillation on the microplate reader. The cell activity was recorded and calculated.

MiR-128-2-5p target gene prediction and dual luciferase reporter assay

The target gene of miR-128-2-5p was predicted using the PicTar (www.pictar.org), TargetScan (<http://www.targetscan.org>), and a database (www.mirbase.org). In 24-well plates, 1×10^5 RAW264.7 macrophages were cultured for 24 h. RAW264.7 macrophages were transfected with the wild type (WT) Tollip 3'-UTR, or the mutant Tollip 3'-UTR was cloned into the p-miR-reporter plasmid (Thermo Fisher Scientific, Inc.) together with miR-128-2-5p mimics, inhibitor, or NC by using Lipofectamine RNAi Max (Thermo Fisher Scientific, Inc.). The cells were cultured at 37°C for 48 h, and the

luciferase activities were measured using a dual-luciferase reporter kit (Promega Corporation, USA).

Experimental animals

Eighty adult male Sprague Dawley rats weighing 251 ± 23 g were purchased from the Kunming Medical University Laboratory Animal Center (Kunming, China). All rats were housed in the Kunming Medical University Animal Care Facility and maintained in pathogen-free conditions. The rats were 8–9 wk of age at the initiation of the experiment and maintained on a standard laboratory food intake. Water was provided *ad libitum*. The environment was maintained at a relative humidity of 30%–70%, temperature of $23^\circ\text{C} \pm 2^\circ\text{C}$, and a 12 h/12 h light/dark cycle. All experiments were approved and performed in accordance with the guidelines of the Animal Care Committee of Kunming Medical University. All experiments were approved by the Ethics Committee of Dali University (Dali, China; Approval number: TCM-2017-041-E17) and performed in accordance with The Guidelines of the Animal Care Committee of Dali University.

Taurocholate-induced SAP

The SAP models were prepared in accordance with the method described by Aho et al.²⁸ Before surgery, the rats were fasted for 12 h and drank freely, anesthetized using the intraperitoneal injection of 1% sodium pentobarbital (50 mg/kg; Shanghai Jixing Biotechnology Co., Ltd Shanghai, China), routinely disinfected, draped, incised into the abdomen along the white line of the abdomen, and retrogradely injected with 5% sodium taurocholate (35 mg/kg) through the pancreaticobiliary duct for about 10 min. The pancreatic tissue pathological examination showed swelling, spotting hemorrhage, and necrosis, which confirmed that the model was successfully prepared. The animals in the sham operation (SO) group retrogradely injected with an equal amount of normal saline through the pancreaticobiliary duct. The SO animals were subjected to the same surgical procedures.

MiR-128-2-5p knockdown by using locked nucleic acid (LNA)-modified anti-miR-128-2-5p

As described previously,²⁹ LNA-modified scrambled or anti-miR-128-2-5p oligonucleotides (Exiqon, Woburn, MA, USA) were diluted in 5 mg/ml saline and administered intraperitoneally at 10 mg/kg for at least 30 min to construct the miR-128-2-5p-knockdown rats. The taurocholate-induced pancreatitis model (model group, $n = 10$) and the SO groups ($n = 10$) were established, and the miR-128-2-5p-knockdown rats were used to establish the miR-128-2-5p model ($n = 10$) and the miR-128-2-5p SO ($n = 10$) rats. The rats were subjected to taurocholate-induced SAP for

24 h, anesthetized using intravenous pentobarbital sodium (50 mg/kg), and sacrificed via cervical dislocation. Their lung tissues were obtained and subjected to real-time PCR, Western blot, and hematoxylin and eosin (H&E) staining to observe the pathological changes in the lung tissues.

Animal groups and drug administration

The rats were randomly assigned into four groups ($n = 10$ for each group), namely, SO, SO treatment, SAP, and SAP treatment groups. Subsequently, as previously described,^{30,31} the SO treatment and the SAP treatment groups were intraperitoneally injected with 20 mg/kg NG-R1 injection 2 h before pancreatitis was induced by taurocholate. The injection was administered once every 12 h. The SO and the model groups were given the same volume of saline by intraperitoneal injection. Then, 48 h after duct infusion or SO, the animals were sacrificed through cervical dislocation and anesthetized with 1% pentobarbital sodium (50 mg/kg body mass; Wuhan Dinghui Chemical Co., Ltd, Wuhan, China). Samples were extracted for investigation. Blood (5 ml) was collected through the cardiac puncture by using heparinized syringes, centrifuged at 4000 g for 10 min, and stored at 4°C for further analysis. The lungs were carefully isolated and weighed for subsequent experiments. The tissues for histological examination were isolated, fixed in 10% formalin, and embedded in paraffin for sectioning. The right upper lobes were utilized to quantify the magnitude of the pulmonary edema, whereas the right lower lobes were used for the histological evaluation.

Collection of the bronchoalveolar lavage fluid (BALF) and tissue samples

After the rats were euthanized, their trachea was isolated, and the right bronchial tube was ligated. The BALF was obtained by placing a 20-gauge catheter into the trachea, through which 3 ml cold PBS was flushed back and forth three times. The BALF was centrifuged at 3000 g for 20 min at 4°C. The protein concentration of the cell-free BALF from all groups was measured using the Bio-Rad protein assay kit and used as an indicator of endothelial and epithelial permeability. The right middle lung lobes were stored in liquid nitrogen at -80°C until subsequent analysis.

qRT-PCR

Prior to RNA extraction, the lung samples were homogenized in the TRIzol reagent (Invitrogen) by using the Mixer 301. The total RNA was extracted in accordance with the manufacturer's instructions. The RNA samples were electrophoresed in agarose gels and visualized using ethidium bromide for quality control. RNA (3 μ g) was reverse transcribed with reverse transcriptase for 1 h at

37°C for the cDNA synthesis. The quantitative changes in the mRNA expression were assessed using qRT-PCR (Bio-Rad CFX) and the SYBR-Green detection, which consisted of SYBR-Green PCR Master Mix (Aria, Tous, Iran). The PCR Master Mix comprised 0.5 units Taq polymerase, 2 μ l of each primer, and 3 μ l of each cDNA sample at a final volume of 20 μ l. Amplifications were repeated thrice. Oligonucleotide primer sequences or specific reverse transcription primers (miR-128-2-5p) are provided in Table 1. β -Actin was used as an endogenous control. Each sample was normalized based on its β -actin content, and the U6 served as an internal normalization standard of miR-128-2-5p. The relative quantification was performed using the $2^{-\Delta\Delta CT}$ method.^{32,33} Following preincubation at 95°C for 10 min, PCR was performed as follows: 35 cycles of denaturation at 95°C for 15 s, annealing at 60°C for 5 s, and elongation at 72°C for 12 s. The experiment was independently repeated thrice.

Western blot

The lung tissues were homogenized in the lysis buffer containing protease inhibitors, and the protein concentrations were determined using the Bradford reagent (Bio-Rad Laboratories Inc., Hercules, CA, USA). Samples were subjected to SDS-PAGE. After electrophoresis at 120 V for 90 min, the separated proteins were transferred onto polyvinylidene difluoride membranes (GE Healthcare, Little Chalfont, Buckinghamshire, United Kingdom) through the wet transfer method (250 mA, 90 min). Nonspecific sites were blocked using 5% nonfat dry milk in TBS with Tween 20 (25 mM Tris, pH 7.5, 150 mM NaCl, and 0.1% Tween 20) for 1 h. The blots were incubated overnight at 4°C with the following: anti-HMGB1 and -Tollip Abs (Cell Signaling Technology Inc.); anti-TLR4, -MyD88, -p-IL-1 receptor-related kinases (IRAK1), and -IRAK1 Abs (Cell Signaling Technology Inc.); anti-NF- κ B65 and -p-I κ B- α Abs (Cell Signaling Technology Inc.); and anti-ERK1 and -p-ERK1 Abs (Cell Signaling Technology Inc.). Anti-rabbit or anti-mouse HRP-conjugated IgG Abs were used to detect the binding of the Abs. The membranes were stripped and reblotted using an anti-actin Ab (Sigma-Aldrich) to normalize the protein loading on each lane. The binding of specific Abs was visualized by exposing the membranes to photographic film after treatment with enhanced chemiluminescence system reagents (GE Healthcare). Quantitative analysis was performed using the Image J. The experiment was independently repeated three times.

Determination of NF- κ B65 and TLR4 activation by using immunohistochemistry

Immunostaining was performed on the lung sections after Ag retrieval by using the Retrieval A (Zymed, South San Francisco, CA) at 100°C for 20 min, and endogenous

Table 1. Primer sequences for genes.

Gene	Primer	Product length (bp)
miR-128-2-5p	F-5'- TCCGATCACAGTGAACCGGT 3' R-5'- GTGCAGGGTCCGAGGT-3'	143 bp
U6	F-5' CTCGCTTCGGCAGCACACA-3' R-5'- AACGCTTCACGAATTTGCGT-3'	158 bp
HMGB1 mRNA	F-5' - TGGTACATATCGGGCTAGAAG -3' R-5'- CCA TACTGTACCAGGCAAGGT-3'	218 bp
TLR4 mRNA	F-5'- CCAAGAACCTAGATCTGAGCTTCAATC-3' R-5'-TCCTGGCTGGACTTAAGCTGTAG-3'	205 bp
Tollip mRNA	F-5'- GGACAACGGTCAGCGACGCA-3' R-5'-CATAGCCCAGACGCAGGCGG-3'	248 bp
NF-κB 65mRNA	F-5'-GGATGGCTACTATGAGGCTGAC-3' R-5'-CTAATGGCTTGCTCCAGGTCTC -3'	171 bp
IκB mRNA	F-5'-GCCTGGACTCCATGAAAGAC-3' R-5'-CAAGTGGAGTGGAGTCTGCTGCAGCTTGTT-3'	277 bp
ERK1 mRNA	F-5'- AACCTGCTCATCAACACCAC-3' R-5'- CGTAGCCACATACTCCGTCA -3'	174 bp
β-Actin	F-5'- AGCGGTTCCGATGCCCT-3' R-5'-AGAGGTCTTTACGGATGTCAACG-3'	190 bp

peroxidases were quenched with 3% H₂O₂. Sections were blocked with 2% BSA in PBS and stained using primary anti-NF-κB65 and TLR4 (Bioworld Technology, Inc., St. Louis Park, MN, USA) at room temperature for 1 h. then sections were washed and applied with the secondary Ab (R&D Systems Minneapolis, MN, USA). The tissues were developed using the Vectastain ABC (Vector Labs, Burlingame, CA) and 3,3'-diaminobenzidine (Vector Labs). NF-κB65- and TLR4-positive expression in the lung tissue was determined and expressed as positive units by using the Image-Pro Plus image analysis software (Media Cy Bematics American Company).

Determination of the BALF and RAW264.7 macrophage cytokines by ELISA

The Nalgene Nunc MaxiSorp plates were coated with a primary Ab against either IL-6, TNF-α, IL-1β, and ICAM-1 in the serum or in BALF (R&D systems) for 1 h at room temperature and then washed with PBS and 0.5% Tween 20. The samples were blocked using casein, seeded into plates for 1 h at room temperature, washed, and applied with biotinylated secondary Ab for 1 h and streptavidin-HRP conjugate (Jackson ImmunoResearch, West Grove, PA) diluted at 1:20,000. The reaction was developed with 0.01% tetramethylbenzidine dissolved in dimethyl sulfoxide and 0.5% H₂O₂, and the absorbance was measured using the endpoint spectrometry.

Determination of the myeloperoxidase (MPO) activity

Lung tissues were transected into small pieces and homogenized on ice by using normal saline. As described

previously³⁴ the MPO activity was determined using the MPO kit produced by Jiancheng Bioengineering Institute (Nanjing, China) in accordance with the manufacturer's instructions.

Determination of the albumin concentration in the BALF

The albumin content in the BALF supernatants was assessed using ELISA for albumin (E91028Mu, USCN Life Science, Wuhan, China). The absorbance was measured at 450 nm/540 nm by using a microplate reader (Infinite 200, Tecan Group, Switzerland).

Detection of pulmonary edema

The total lung water (TLW) content was measured as previously described to quantify pulmonary edema.³⁵ The left lung was isolated for the TLW content determination. The lung was weighed using an automatic electric balance (Sartorius, Göttingen, Germany), oven dried at 80°C for 48 h, and re-weighed to obtain its dry mass. The TLW content was calculated as follows: TLW content=(wet lung mass – dry lung mass)/dry lung mass.

Lung histopathology

The middle lobe of the right lung was fixed by infusing 10% formaldehyde solution at the same pressure, and the inflation of the lung was kept uniform. Then, the lung tissue was embedded in paraffin wax, transected, and stained with H&E. The pathological tissue changes were observed using optical microscopy. The lung injury based on the

infiltration of inflammatory cells, pulmonary interstitial and alveolar edema, damage to alveolar structure, and degree of fibrosis was assessed using the grading system reported by Szapiel et al.³⁶ As described previously,³⁷ ALI was scored as follows: (i) alveolar congestion, (ii) hemorrhage, (iii) infiltration or aggregation of neutrophils in airspace or vessel wall, and (iv) thickness of alveolar wall/hyaline membrane formation. Each item was scored on a five-point scale as follows: 0, minimal damage; 1, mild damage; 2, moderate damage; 3, severe damage; and 4, maximal damage. Repeatedly measured data were statistically analyzed using analysis of variance (ANOVA).

Statistical analysis

The SPSS 11.0 software was used for the statistical analysis of the results. Data were expressed as mean \pm SD unless indicated otherwise. Data were analyzed using ANOVA and the Newman–Keuls comparison. For two-group comparisons, the unpaired Student's *t*-test was used (GraphPad Software, San Diego, CA). $P < 0.05$ was considered statistically significant.

Results

Transfection efficiency of the mimics or the inhibitor

MiR-128-2-5p mimics, miR-128-2-5p mimic-NC, miR-128-2-5p inhibitor, and miR-128-2-5p inhibitor-NC were mixed with Lipofectamine RNAi Max (Thermo Fisher Scientific, Inc.) and subsequently added to the RAW264.7 macrophage cultures to observe the transfection efficiency of the mimics, control, or inhibitor. Cultures were transfected for 24 h, and the miR-128-2-5p level was measured using qRT-PCR. The miR-128-2-5p levels in the mimics (1.06 ± 0.25) increased compared with those in the mimic-NC (0.39 ± 0.16), as shown in Figure 1. Moreover, the miR-128-2-5p levels in the inhibitor (0.41 ± 0.19) considerably decreased compared with those in the inhibitor-NC (0.17 ± 0.08). The mimics or inhibitor was successfully transfected.

Significant attenuation of the Tollip signaling pathway in RAW264.7 macrophages by miR-128-2-5p

The Tollip signaling pathway is one of the major pathways of ALI and inflammatory reaction. miR-128-2-5p mimics, miR-128-2-5p mimic-NC, miR-128-2-5p inhibitor, and miR-128-2-5p inhibitor-NC were mixed with Lipofectamine 2000 (Invitrogen) and added to the cell culture to investigate the effect of miR-128-2-5p on the Tollip signaling pathway in the RAW264.7 macrophages. The cultures were transfected for 24 h, and the expression levels of NF- κ B65, p-I κ B- α , TLR4, and Tollip were measured using Western blot. As shown in Figure 1, the

miR-128-2-5p expression in the miR-128-2-5p inhibitor was down-regulated and further decreased NF- κ B65, p-I κ B- α , and TLR4 expression levels (Figures 2(A)–2(C)). Conversely, miR-128-2-5p expression in the miR-128-2-5p mimics was up-regulated; decreased the Tollip protein expression; and evidently increased NF- κ B65, p-I κ B- α , and TLR4 expression levels (Figures 2(A)–2(C)). Therefore, miR-128-2-5p may regulate the Tollip anti-inflammatory signaling pathways.

Significant increase in cellular inflammation and cell viability of RAW264.7 macrophages by miR-128-2-5p

MiR-128-2-5p mimics, miR-128-2-5p mimic-NC, miR-128-2-5p inhibitor, and miR-128-2-5p inhibitor-NC were mixed with Lipofectamine 2000 (Invitrogen) and then added to the cell culture to observe the effect of miR-128-2-5p on the cellular inflammation and the cell viability of the RAW264.7 macrophages. The cultures were transfected for 24 h, and IL-6 and TNF- α levels were measured using ELISA. The cell viability was measured using the CCK-8 assay. As shown in Figure 2, miR-128-2-5p expression in the miR-128-2-5p mimics significantly increased the production of IL-6 and TNF- α in RAW264.7 macrophages (Figures 2(D) and 2(E)) and increased the cell viability (Figure 2(F)). Conversely, miR-128-2-5p expression in the miR-128-2-5p inhibitor significantly decreased the production of IL-6 and TNF- α in RAW264.7 macrophages (Figures 2(D) and 2(E)) and decreased their cell viability (Figure 2(F)). Therefore, miR-128-2-5p expression can promote the intracellular inflammation and the cell viability.

Effect of NG-R1 treatment on miR-128-2-5p and Tollip signaling pathway in RAW264.7 macrophages

RAW264.7 macrophages were incubated with LPS (1 mg/L) and various concentrations of NG-R1 (10, 20, 30, 40, and 50 μ M) for 24 h. The effects of NG-R1 on LPS-induced miR-128-2-5p and the Tollip signaling pathway in RAW264.7 macrophages were analyzed. The expression of miR-128-2-5p was measured using qRT-PCR, and the expression levels of Tollip, NF- κ B65, p-I κ B- α , and TLR4 were measured using Western blot. As shown in Figure 3, LPS evidently increased the miR-128-2-5p expression, decreased the Tollip expression, and increased NF- κ B65, p-I κ B- α , and TLR4 expression levels in RAW264.7 macrophages. However, the NG-R1 treatment evidently decreased miR-128-2-5p expression, increased Tollip expression, and decreased NF- κ B65, p-I κ B- α , and TLR4 expression levels in these cells in a concentration-dependent manner.

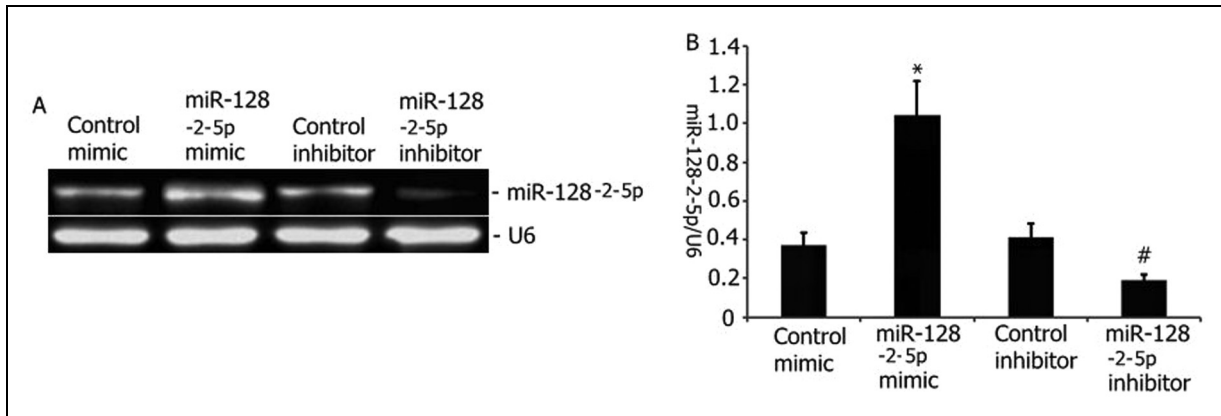


Figure 1. Transfection efficiency of the mimics or inhibitor. MiR-128-2-5p mimics, miR-128-2-5p mimic-NC, miR-128-2-5p inhibitor, and miR-128-2-5p inhibitor-NC were mixed with Lipofectamine 2000 (Invitrogen) and added to the A549 cell culture. The cultures were transfected for 24 h, and the miR-128-2-5p level was measured using qRT-PCR. The data obtained from quantitative densitometry are presented as mean \pm SD of three independent experiments. The data from three independent experiments are presented as mean \pm SD. * $P < 0.05$ vs control mimic. # $P < 0.05$ vs control inhibitor.

Effect of NG-R1 treatment on cellular inflammation and cell viability of LPS-induced RAW264.7 macrophages

RAW264.7 macrophages were incubated with LPS (1 mg/l) and various concentrations of NG-R1 (10, 20, 30, 40, and 50 μ M) for 24 h, and the effects of the NG-R1 on cellular inflammation and cell viability were analyzed. The IL-6 and the TNF- α levels were measured using ELISA, and the cell viability was determined using the CCK-8 assay. As shown in Figure 4, the LPS evidently increased the secretion of IL-6 and TNF- α and cell viability in the RAW264.7 macrophages. However, NG-R1 treatment evidently decreased the secretion of IL-6 and TNF- α and the cell viability in a concentration-dependent manner.

Amelioration of SAP-induced ALI by miR-128-2-5p knockdown

A miR-128-2-5p knockdown construct was introduced to rats by intravenous tail administration of anti-miR-128-2-5p oligonucleotides to analyze the effect of miR-128-2-5p knockdown on SAP-induced ALI through the intraperitoneal taurocholate challenge. H&E staining was performed. As shown in Figure 3, the histopathological examination of the lungs of taurocholate-treated miR-128-2-5p-knockdown rats revealed a markedly decreased inflammatory cell infiltration and lung injury score compared with the WT animals (Figures 5(A) and 5(B)).

Enhancement of Tollip expression and attenuation of lung inflammation in acute pancreatitis-induced acute lung tissue by miR-128-2-5p knockdown

The miR-128-2-5p knockdown model was constructed through the intravenous tail administration of

anti-miR-128-2-5p oligonucleotides and treatment with intraperitoneal taurocholate challenge. The effect of the miR-128-2-5p on the Tollip expression in acute pancreatitis-induced acute lung tissue was observed. The miR-128-2-5p expression was measured using qRT-PCR. The NF- κ B, HMGB1, TLR4, and Tollip protein expression levels in acute pancreatitis-induced lung tissue were measured using Western blot. As shown in Figure 6, the miR-128-2-5p knockdown significantly reduced the miR-128-2-5p expression; increased the Tollip expression; reduced the NF- κ B, p-I κ B- α , HMGB1 and TLR4 expression levels in the lung tissue; and decreased the lung IL-6 and TNF- α levels.

Tollip as a direct target of miR-128-2-5p

The mediation of miR-128-2-5p on the ALI inflammatory response was investigated. According to well-known databases for miRNA target prediction, Tollip, an important pro-inflammatory regulator of acute pancreatitis, is one of the candidate targets of the miR-128-2-5p. In the current study, the mRNA and the protein levels of Tollip dramatically decreased after miR-128-2-5p overexpression (Figures 7(A)–7(D)). The WT and the mutant Tollip were constructed for the dual luciferase reporter assay to confirm the interaction between Tollip and miR-128-2-5p (Figures 7(E) and 7(F)). As hypothesized, the miR-128-2-5p bound to WT Tollip 3'-UTR but not to mutant Tollip 3'-UTR (Figures 7(E) and 7(F)).

Effect of NG-R1 treatment on the expression of miR-128-2-5p in acute pancreatitis-induced rat lung tissues

MiR-128-2-5p expression was determined using qRT-PCR to investigate the effect of NG-R1 treatment on the

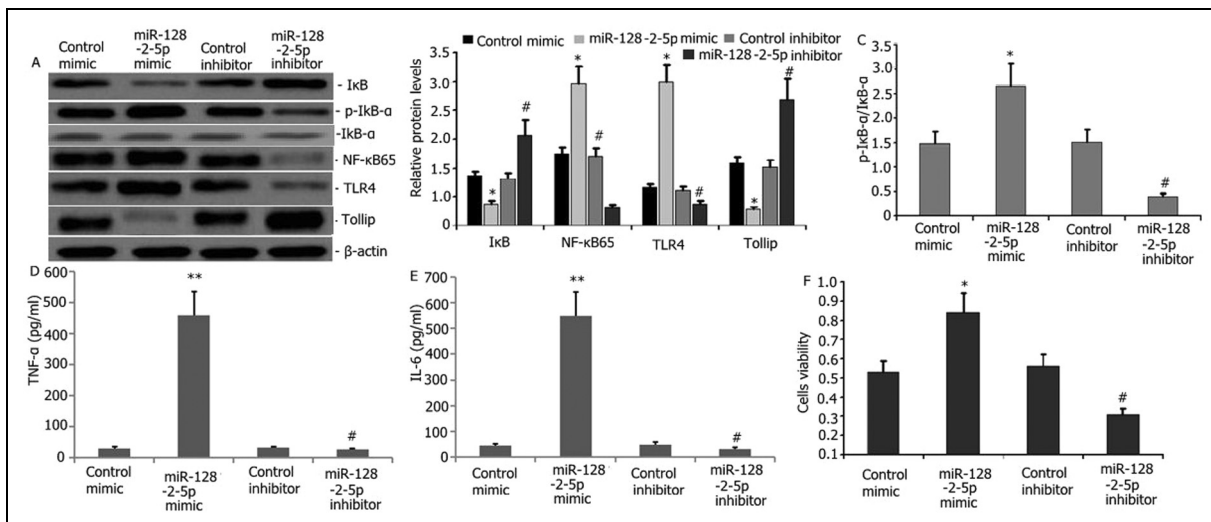


Figure 2. Effect of miR-128-2-5p on the tollip signaling pathway in RAW264.7 macrophages. MiR-128-2-5p mimics, miR-128-2-5p mimic-NC, miR-128-2-5p inhibitor, and miR-128-2-5p inhibitor-NC were mixed with Lipofectamine 2000 (Invitrogen) and added to the cell culture. The cultures were transfected for 24 h. (A–C) Expression levels of NF-κB65, p-IκB-α, TLR4, and Tollip were measured using Western blot. (D–E) IL-6 and TNF-α expression levels in RAW264.7 macrophages were measured using ELISA. (F) The growth inhibition rate was measured using the MTT assay. The data obtained from quantitative densitometry are presented as mean ± SD of three independent experiments. * $P < 0.05$ vs control mimic. # $P < 0.05$ vs control inhibitor.

expression of miR-128-2-5p in acute pancreatitis-induced rat lung tissues. As shown in Figure 8, NG-R1 treatment decreased the expression of the miR-128-2-5p in acute pancreatitis-induced rat lung tissues (Figures 8(A) and 8(B)).

Effect of NG-R1 treatment on expression levels of ERK1, Tollip, HMGB1, TLR4, IκB, and NF-κB genes in rat tissues with acute pancreatitis-induced ALI

qRT-PCR was used to measure the expression levels of ERK1, Tollip, HMGB1, TLR4, IκB, and NF-κB genes in

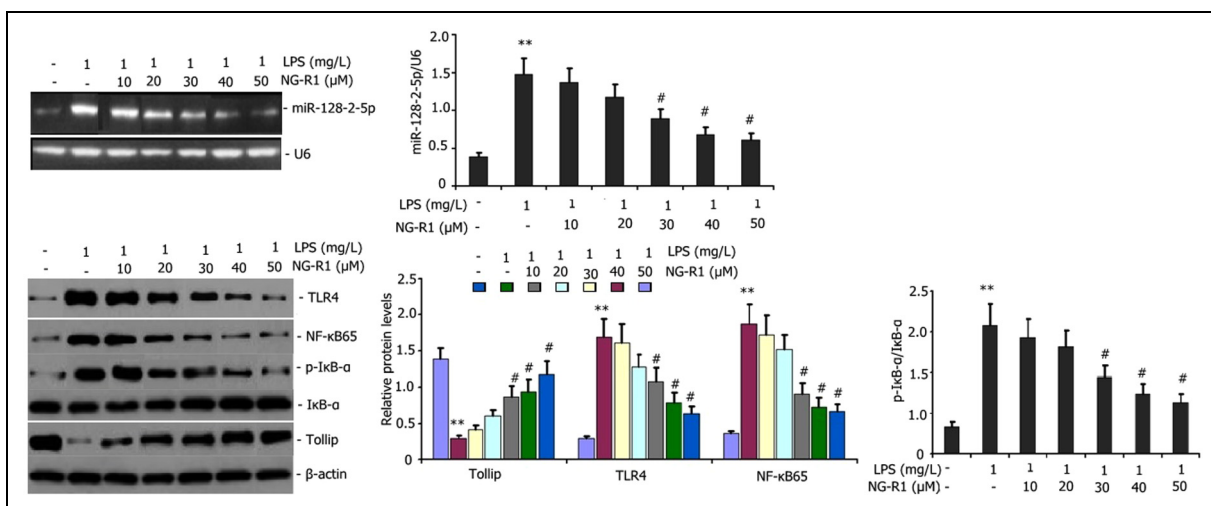


Figure 3. Effect of NG-R1 on miR-128-2-5p and the tollip signaling pathway in RAW264.7 macrophages. RAW264.7 macrophages were incubated with LPS (1 mg/l) and various concentrations of NG-R1 (10, 20, 30, 40, and 50 μM) for 24 h to analyze the effects of NG-R1 on LPS-induced miR-128-2-5p and the Tollip signaling pathway in RAW264.7 macrophages. The miR-128-2-5p expression was measured using qRT-PCR. The expression levels of Tollip, NF-κB65, p-IκB-α, and TLR4 were measured using Western blot. The data obtained from quantitative densitometry are presented as mean ± SD of three independent experiments. ** $P < 0.01$, * $P < 0.05$ vs blank control group. # $P < 0.05$ vs LPS group.

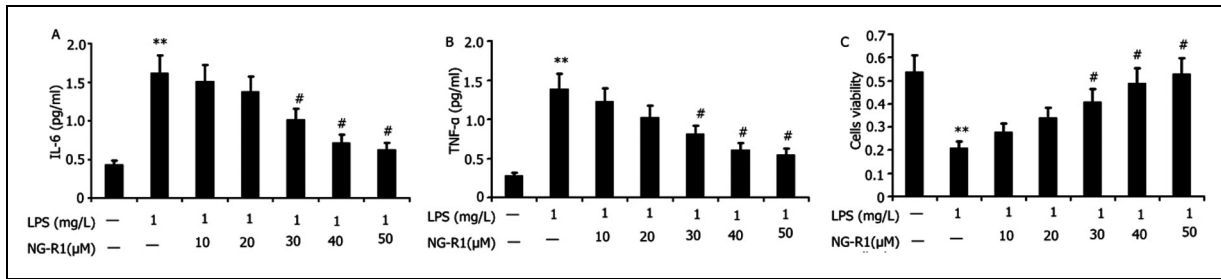


Figure 4. Effect of NG-R1 on cellular inflammation and cell viability of LPS-induced RAW264.7 macrophages. RAW264.7 macrophages were incubated with LPS (1 mg/l) and various concentrations of NG-R1 (10, 20, 30, 40, and 50 μM) for 24 h to analyze the effect of NG-R1 on cellular inflammation and cell viability of LPS-induced RAW264.7 macrophages. IL-6 and TNF-α levels were measured using ELISA. The cell viability was measured using the CCK-8 assay. Data are expressed as mean ± SD of three replicates. ** $P < 0.01$ vs the blank control group; # $P < 0.05$ vs the LPS group.

pancreatitis-induced lung tissues. The *Tollip*, *HMGB1*, *TLR4*, *ERK1*, and *NF-κB* expression levels markedly increased, and the *IκB* expression was significantly down-regulated after acute pancreatitis-induced ALI (Figures 8(A) and 8(C)). After the application of NG-R1 therapy, the *IκB* expression was markedly enhanced, whereas the *Tollip*, *HMGB1*, *TLR4*, *ERK1*, and *NF-κB* expression levels were significantly reduced (Figures 8(A) and 8(C)). Therefore, NG-R1 treatment could suppress the *Tollip*, *HMGB1*, *TLR4*, *ERK1*, and *NF-κB* gene expression and up-regulate the *IκB* gene expression (Figures 8(A) and 8(C)).

Effect of NG-R1 treatment on protein expression levels of *Tollip*, *TLR4*, *MyD88*, *p-IRAK1*, *p-ERK1*, *IκB*, *NF-κB65* and *p-ERK1* in rat lung tissues with taurocholate-induced acute pancreatitis

The protein expression levels of *Tollip*, *TLR4*, *MyD88*, *p-IRAK1*, *p-ERK1*, *IκB*, *NF-κB65* and *p-ERK1* were measured using Western blot to observe the effect of NG-R1 treatment on the expression levels of the respective proteins in the lung tissues mediated by the taurocholate-induced acute pancreatitis. The expression levels of *TLR4*, *MyD88*, *p-IRAK1*, *p-ERK1*, *IκB*, *NF-κB65*, *p-ERK1* proteins significantly increased, whereas the expression level of *Tollip* protein significantly decreased in rat lung tissues *in vivo* during taurocholate-induced acute pancreatitis ($P < 0.05$, Figures 8(D)–8(H)). The expression levels of *TLR4*, *MyD88*, *p-IRAK1*, *p-ERK1*, *IκB*, *NF-κB65*, *p-ERK1* protein significantly decreased and the expression level of *Tollip* protein significantly increased in rat lung tissues mediated by the taurocholate-induced acute pancreatitis in response to NG-R1 administration ($P < 0.05$, Figures 8(D)–8(H)).

Attenuation of MPO activity in the rat lungs and pancreas with taurocholate-induced acute pancreatitis after NG-R1 treatment

The MPO activity in the rat lungs and pancreas treated with taurocholate with or without NG-R1 was investigated to

investigate the potential mechanism underlying the protective effect of the NG-R1 on the acute pancreatitis-induced lung and pancreatic injuries. As shown in Figure 9, taurocholate significantly increased the MPO activity in lungs and pancreas at 48 h. These increments were reduced in the treatment group (Figure 9(A)).

Attenuation of the lung inflammation in rats with taurocholate-induced acute pancreatitis by NG-R1 treatment

The BALF was collected at 48 h to evaluate the levels of TNF-α, IL-6, IL-1β and ICAM-1. As shown in Figure 9, acute pancreatitis caused a significant acute systemic inflammatory response, as demonstrated by the increased serum concentrations of the pro-inflammatory mediators TNF-α, IL-6, IL-1β and ICAM-1 proteins (Figures 6(B)–6(E)). The presence of the NG-R1 reduced the increase in these pro-inflammatory cytokines at 24 h (Figures 6(B)–6(E)).

Effect of NG-R1 treatment on the activation of *NF-κB65* and *TLR4* taurocholate- and acute pancreatitis-induced lung tissues

As shown in Figure 10, the lung activation of *NF-κB65* and *TLR4* in the SO group significantly decreased at 48 h (Figures 10(A)–10(D)). However, *NF-κB65* and *TLR4* expression levels were markedly increased in the model and the treatment groups (Figures 10(A)–10(D)). At 48 h after the NG-R1 administration, the activation of *NF-κB65* and *TLR4* was markedly decreased in the treatment group (Figures 10(A)–10(D)).

Reduction of the lung wet/dry mass ratio and the BALF protein concentration in rats with taurocholate-induced acute pancreatitis after NG-R1 treatment

The lung wet/dry mass ratio was significantly increased at 48 h in taurocholate- and acute pancreatitis-induced lung

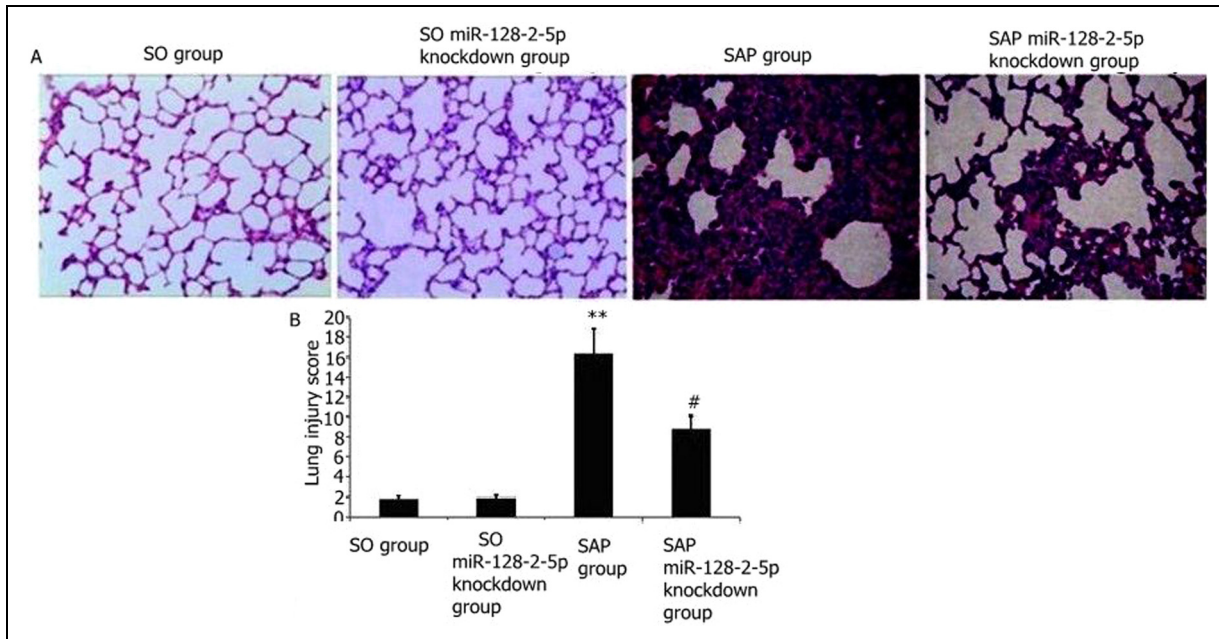


Figure 5. Effect of miR-128-2-5p knockdown on SAP-induced ALI. The miR-128-2-5p-knockdown construct was delivered to rats through intravenous tail administration of anti-miR-128-2-5p oligonucleotides, and SAP-induced ALI was induced through intraperitoneal taurocholate challenge. The rat lungs were histopathologically examined. The lung injury score was measured. (A) Representative images of H&E-stained lung sections from three experimental groups (400× magnification). (B) Lung injury score. Data are expressed as mean ± SD of three experiments. ** $P < 0.01$ vs SO or SO treatment group; ### $P < 0.01$ vs SAP group.

tissues (Figure 11). The NG-R1 treatment significantly attenuated this change (Figure 11). Additionally, in terms of endothelial and epithelial permeability, the BALF protein

concentration quickly increased after taurocholate-induced SAP (Figure 11). The treatment group also exhibited significantly low protein concentrations (Figure 11(D)).

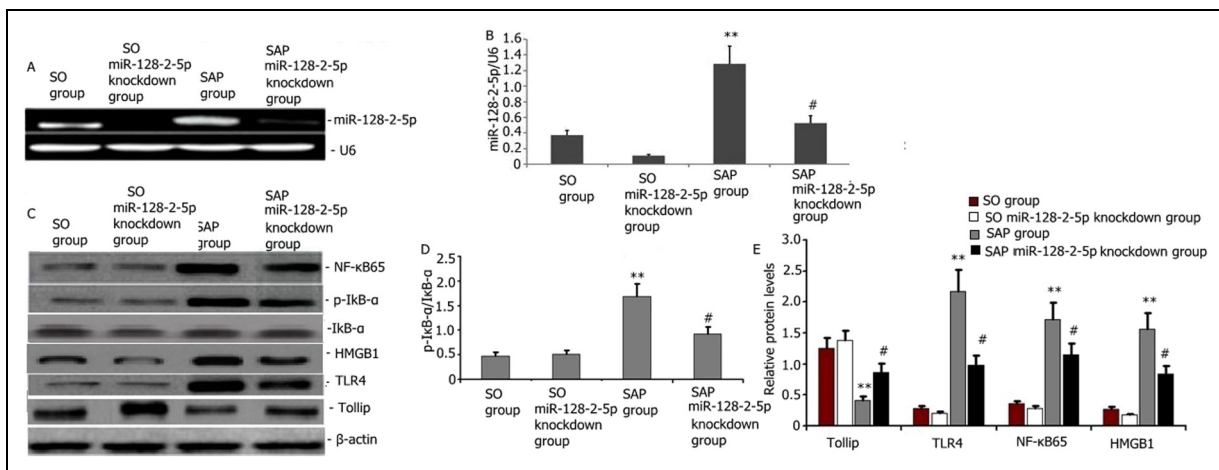


Figure 6. Effect of miR-128-2-5p knockdown on miR-128-2-5p and Tollip/TLR4 signaling pathway in SAP-induced ALI. The miR-128-2-5p-knockdown construct was delivered to rats through intravenous tail administration of anti-miR-128-2-5p oligonucleotides, and SAP-induced ALI was established through intraperitoneal taurocholate challenge. The rat lungs were histopathologically examined. (A–B) Representative qRT-PCR images showing the miR-128-2-5p expression level from four experimental groups. (C–E) Representative Western blots and statistical summary of the densitometric analysis of the expression levels of NF-κB5, p-IκB-α, HMGB1, TLR4, and Tollip in rat lungs with acute pancreatitis at 24 h after administering NG-R1 treatment. Data were expressed as mean ± SD of three experiments. ** $P < 0.01$ vs SO group; # $P < 0.05$ vs SAP group.

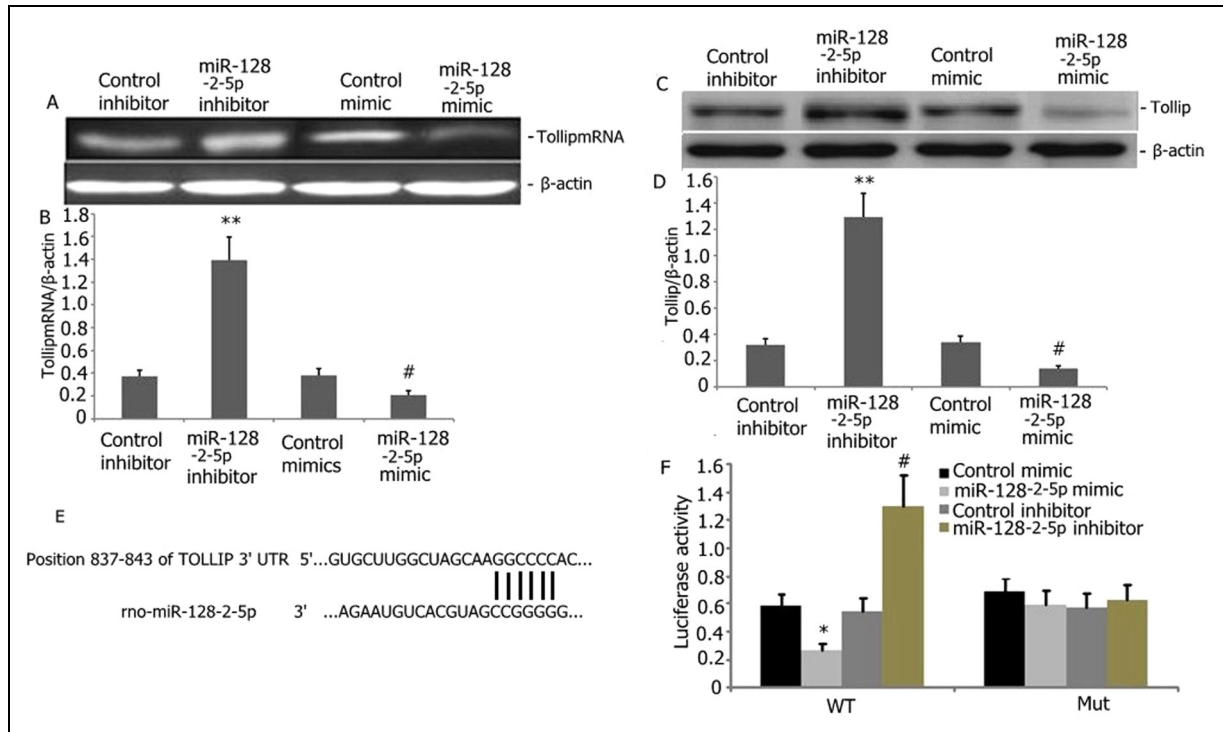


Figure 7. Tollip as a direct target of miR-128-2-5p. (A–B) Tollip mRNA levels increased with miR-128-2-5p down-regulation in RAW264.7 macrophages ($P < 0.05$). (C–D) The Tollip protein levels decreased with miR-128-2-5p overexpression in RAW264.7 macrophages compared with vector controls ($P < 0.05$). MiR-128-2-5p bound to Tollip-3'-UTR-wt, whereas binding was blocked by Tollip-3'-UTR-mt. (F) Dual luciferase reporter assays confirmed that the miR-128-2-5p mimic bound to Tollip-3'-UTR-wt but not to Tollip-3'-UTR-mt ($P < 0.05$).

Amelioration of the acute pancreatitis-induced histological ALI after NG-R1 administration

The histopathological analysis of H&E-stained lung sections was performed to analyze the effect of NG-R1 on the acute pancreatitis-induced histological lung injury. The histological analyses of lungs following taurocholate and acute pancreatitis induction revealed that the capillaries in the lung tissue expanded and became congested by the significant increase in neutrophils (Figures 12(A) and 12(B)). In addition, the lung septa thickened and did not improve after 48 h, and the lung injury score markedly increased (Figures 12(A) and 12(B)). The treatment group also displayed moderate injury. However, the severity of the moderate injury was significantly ameliorated. The lung injury score in the treatment group significantly decreased compared with that in the model group (Figures 12(A) and 12(B)).

Discussion

SAP is highly susceptible to ALI,³⁸ which is the most pertinent manifestation of the extra-abdominal organ dysfunction in SAP and an important cause of extremely early mortality (in the first week) during the course of SAP.³⁹ High concentrations of inflammatory mediators and the

activation of inflammatory cells play an important role in ALI's initiation and progression.^{39–41} In the current study, rats with SAP induced by taurocholate generally had poor condition and exhibited shortness of breath, evident wheezing, low activity, and cyanosis around the limbs, mouth, nose, and tachypnea. Increased MPO activity and increased production of TNF- α , IL-6, and ICAM-1 pro-inflammatory mediators in BALF were also found. H&E staining showed significant pulmonary hemorrhage, massive neutrophil infiltration, alveolar septal thickening, alveolar dilatation, and thrombosis in pulmonary capillaries. After the SAP was induced by taurocholate, the lungs were clearly inflamed, and the exudation of the lungs and the lung injury were severe. The pathological lung injury score was significantly increased, thereby conforming to the pathological features of ALI induced by acute pancreatitis.

Currently, no specific treatment exists for ALI. However, the PNS 1 has been used in treating inflammation-related diseases with some therapeutic effects.⁴² In this study, the treatment with *Panax* NG-R1 reduced MPO activity in the lung tissues, the levels of TNF- α , IL-6, and ICAM-1 pro-inflammatory mediators in the BALF, the lung wet/dry mass ratio, the alveolar lavage fluid protein concentration, neutrophil infiltration, and the H&E staining after dissection in the thoracic cavity.

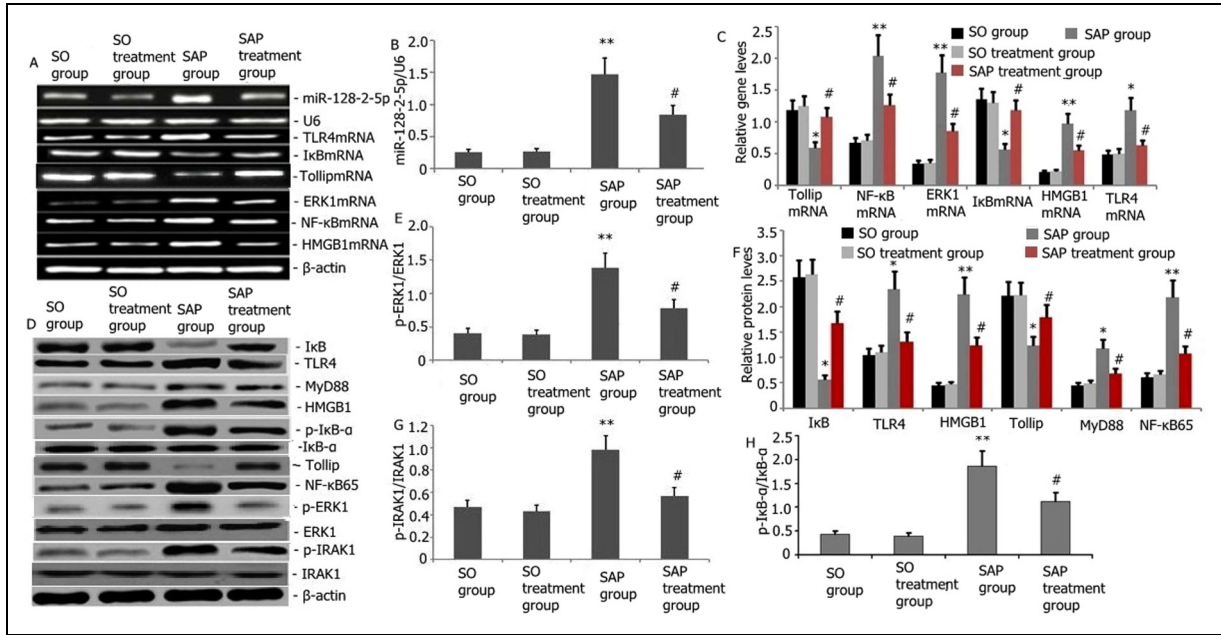


Figure 8. Effect of the notoginsenoside R1 treatment on the gene and the protein expression levels of miR-128-2-5p, ERK1, Tollip, HMGB1, TLR4, IkB, and NF-κB from the acute pancreatitis-induced lung tissue. (A) Representative qRT-PCR images showing the miR-128-2-5p, *IkB*, *ERK1*, *Tollip*, *HMGB1*, *TLR4*, and *NF-κB* genes expression level in rats' lungs at 48 h after the notoginsenoside R1 administration. (B–C) Statistical summary of the densitometric analysis of the expression levels of *miR-128-2-5p*, *ERK1*, *Tollip*, *HMGB1*, *TLR4*, and *NF-κB* genes in rats. (D) Representative Western blots showing the expression levels of TLR4, p-IRAK1, MyD88, Tollip, p-ERK1, NF-κB65, IkB, p-IkB-α and HMGB1 in rats' lungs with acute pancreatitis at 24 h after the notoginsenoside R1 administration. (E–H) Statistical summary of the densitometric analysis of the expression levels of TLR4, p-IRAK1, MyD88, Tollip, p-ERK1, NF-κB65, IkB, p-IkB-α, and HMGB1 in rat lung tissues. Data were presented as mean \pm SD of three independent experiments. * $P < 0.05$, ** $P < 0.01$ vs. the SO group; # $P < 0.05$, ### $P < 0.01$ vs. the SAP group.

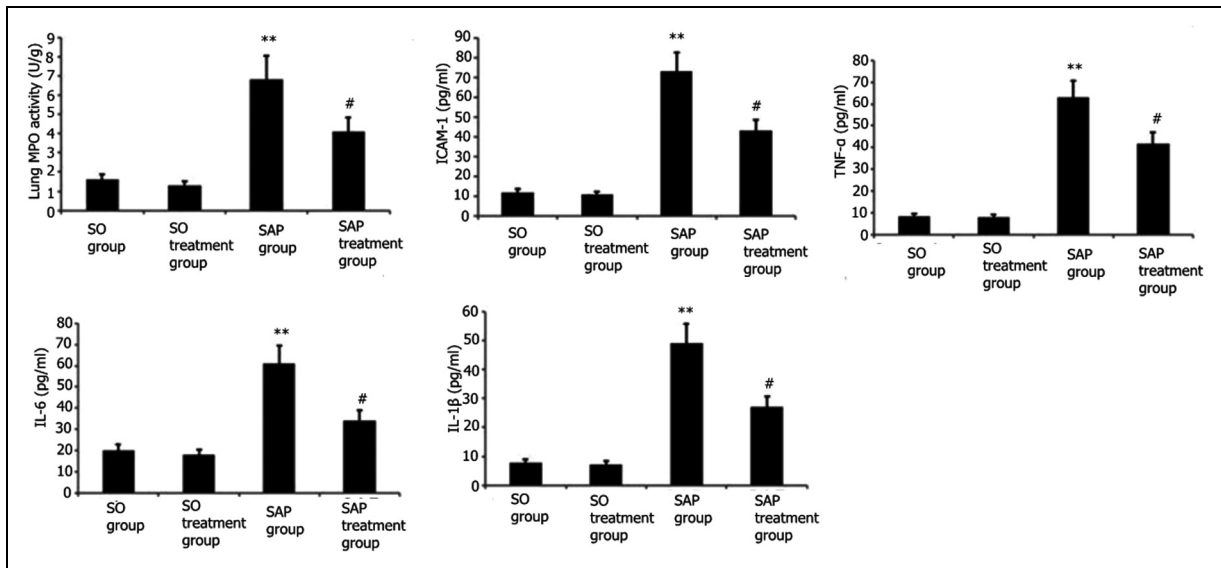


Figure 9. Attenuation of MPO activity and systemic inflammation in the lungs and pancreas in acute pancreatitis-induced lung injury by NG-R1 treatment. (A) The MPO activity in the lungs and pancreas were measured at 48 h after NG-R1 administration. (B–F) The BALF TNF-α, IL-1β, IL-6, and ICAM-1 levels were determined using ELISA at 48 h after NG-R1 administration. Data are expressed as mean \pm SD. ** $P < 0.01$ vs SO group; # $P < 0.05$ vs SAP group.

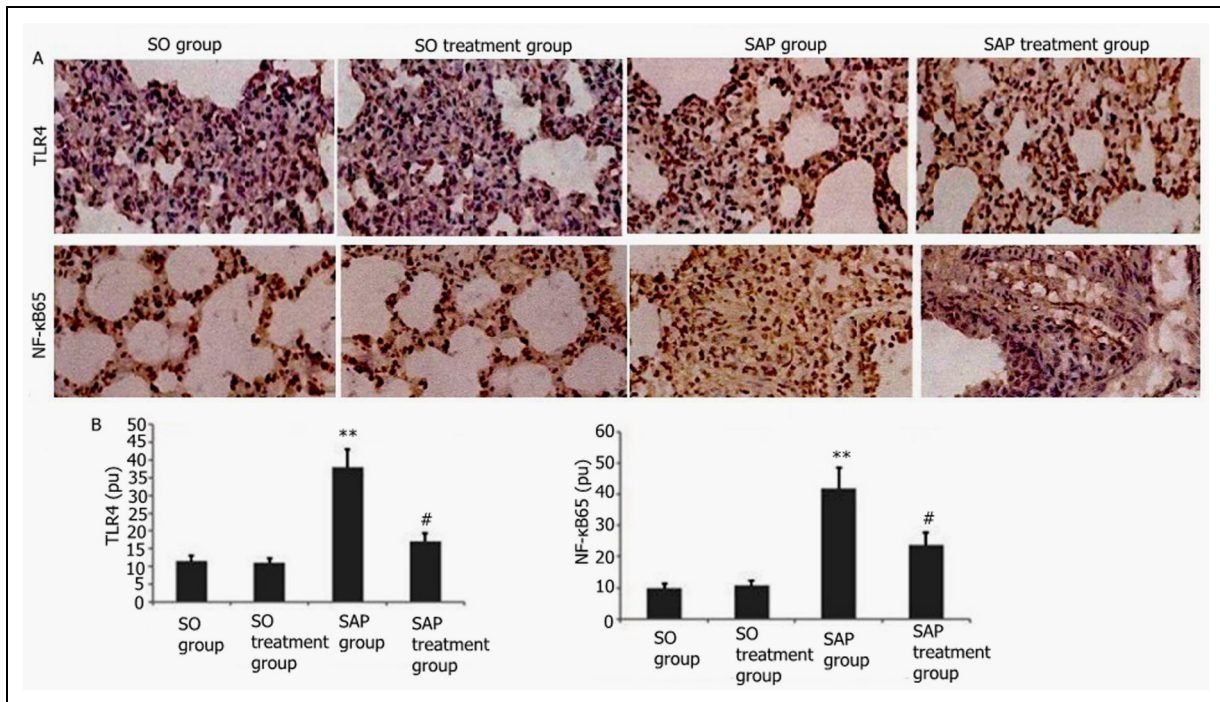


Figure 10. Effect of NG-R1 on the activation of NF- κ B65 and TLR4 in acute pancreatitis-induced lung tissue observed using immunohistochemical staining. (A) Representative immunohistochemically stained graphs of NF- κ B65- and TLR4-positive expression (400 \times magnification). (B) Statistical analysis of NF- κ B65- and TLR4-positive expression. Data are expressed as mean \pm SD. ** $P < 0.01$ vs SO group; # $P < 0.05$ vs SAP group.

MiR-128-2-5p has been widely studied in various diseases, such as esophageal squamous cell cancer, lung cancer, and kidney inflammation.^{43–45} In recent studies, miR-128-2-5p was significantly increased, and the T cells and the NF- κ B signaling pathway were activated. However, the down-regulation of miR-128-2-5p expression significantly suppressed the activation of T cells and the NF- κ B signaling pathway, which was mediated by TNFAIP3, further alleviating the RA symptom.²⁵ In the present study, miR-128-2-5p was involved in the development of ALI induced by acute pancreatitis. At the cellular level, the miR-128-2-5p expression increased in the miR-128-2-5p mimic group, promoted the activity of the Tollip signaling pathway, increased the activity of the TLR4/NF- κ B65 signaling pathway, increased the intracellular inflammation, and the growth inhibition rate of the RAW264.7 macrophages. In this study, the miR-128-2-5p knockout with anti-miR-128-2-5p oligonucleotides significantly reduced miR-128-2-5p expression in the lung and decreased Tollip expression, TLR4/NF- κ B65 signaling pathway activity, lung inflammation, and ALI induced by severe pancreatitis. These results suggested that a reduced miR-128-2-5p expression was protective against severe ALI induced by SAP. Therefore, we observed whether PNS 1 could reduce the expression of miR-128-2-5p and ALI induced by SAP. The *Panax* NG-R1 significantly reduced the expression of miR-128-2-5p in SAP-induced

lung tissues and decreased Tollip expression, the TLR4/NF- κ B65 signaling pathway activity, and lung inflammation, thereby improving the ALI induced by SAP.

Previous studies have shown that Tollip overexpression reduced inflammatory symptoms and improved the survival during the mesenteric ischemia/reperfusion injury.^{46,47} Similarly, pre-treatment with the Tollip inducer alleviated hepatic and renal dysfunctions in the experimental model of LPS.⁴⁸ The Tollip protein molecules can exhibit abnormal expression in patients with ulcerative colitis.⁴⁹ *In vivo*, Tollip can inhibit the LPS-stimulated phosphorylation activation of IRAK1 and reduce the NF- κ B transcription.⁵⁰ Increase Tollip expression induced by the non-toxic immunomodulator monophosphoryl lipid A in the medullary thick ascending limb can inhibit the LPS-induced TLR4 signaling by suppressing the activation of IRAK-1, thereby preventing the activation of ERK.⁵⁰ In this study, Tollip expression in ALI induced by SAP significantly decreased, further confirming that the expression levels of HMGB1, TLR4, MyD88, p-IRAK1, NF- κ B65, and p-I κ B- α proteins and of the *HMGB1*, *TLR4*, *IRAK1*, and *NF- κ B65* genes significantly increased. Furthermore, the TLR4 and the NF- κ B65 activities in the lung tissue increased, whereas the HMGB1, MyD88, p-IRAK1, NF- κ B65, and p-I κ B- α proteins were the important signals of the TLR4/MyD88 and the HMGB1/4/TLR4/NF- κ B pathways, suggesting that

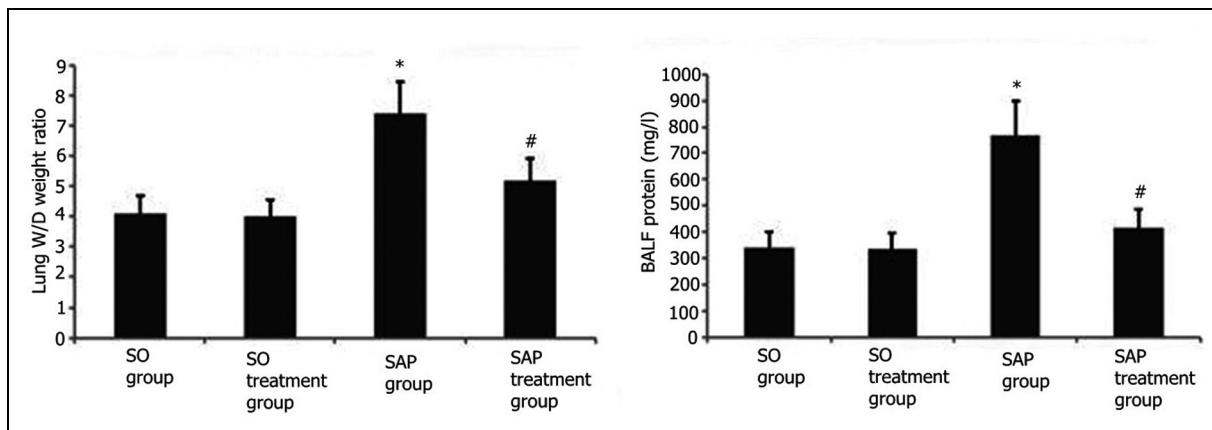


Figure 11. Effect of NG-R1 treatment on the lung wet/dry mass ratio and the BALF protein concentration in rats with taurocholate-induced acute pancreatitis. SAP was induced using intraperitoneal injection of 5% sodium taurocholate. Subsequently, the rats were administered with either 15 mg/kg NG-R1 injection or 300 μ l aqueous saline via tail vein injection for 48 h. Lung wet/dry mass ratio and BALF protein concentration were measured. Data are expressed as mean \pm SEM. ** $P < 0.01$ vs control group; # $P < 0.05$ vs SAP group. Data are expressed as mean \pm SD. * $P < 0.05$ vs SO group; # $P < 0.05$ vs model group.

Tollip might modulate the inflammatory response through the TLR4/MyD88 and HMGB1/TLR4/NF- κ B signaling pathways. Furthermore, administration of NG-R1 significantly increased the Tollip expression and decreased the expression levels of TLR4, MyD88, p-IRAK1, NF- κ B65, and p-I κ B- α proteins in the lungs, suggesting that the *Panax* NG-R1 might block the TLR4/MyD88 and HMGB1/TLR4/NF- κ B signaling pathways to regulate the inflammatory response in the lungs by up-regulating the Tollip pathway.

In this study, miR-128-2-5p up-regulation led to a decrease of the activity of the Tollip pathway and inflammation in RAW264.7 macrophages, and the attenuation and knockdown of miR-128-2-5p in rats with SAP-induced ALI decreased the inflammation and increased the activity of the Tollip signaling pathway in the lungs. Currently, the potential targets between miR-128-2-5p and Tollip are not identified.²³ We further explored the potential link between miR-128-2-5p and Tollip. The online TargetScan predicted that miR-128-2-5p binds to the Tollip 3'-UTR.

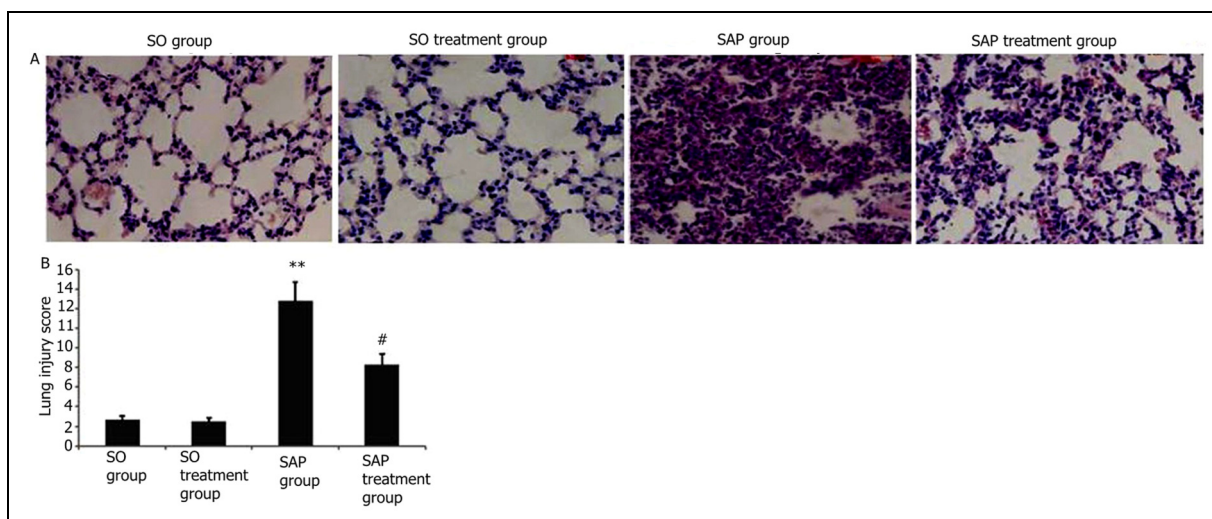


Figure 12. Effect of NG-R1 treatment on the changes in lung pathology and lung injury score in rats with taurocholate-induced acute pancreatitis. SAP was induced using intraperitoneal injection of 5% sodium taurocholate. Subsequently, rats were administered with either 15 mg/kg NG-R1 injection or 300 μ l aqueous saline via tail vein injection for 48 h. (A) Representative images of H&E-stained lung sections from four experimental groups (200 \times magnification). (B) Statistical analysis of lung injury score. Data are expressed as mean \pm SD. ** $P < 0.01$ vs control group; # $P < 0.05$ vs paraquat group. Data are expressed as mean \pm SEM. * $P < 0.01$ vs SO group; # $P < 0.05$ vs SAP group.

The luciferase reporter assay further demonstrated that *Tollip* was a target gene of miR-128-2-5p. The present study was the first to identify the target relationship between *Tollip* and miR-128-2-5p and indicated that miR-128-2-5p mediated the mechanism of ALI by regulating *Tollip* expression. This finding suggested that *Tollip* can mediate its anti-inflammatory effects through the induction of miR-128-2-5p. Therefore, this experiment demonstrated that the PNS 1 regulated the intrapulmonary inflammatory response induced by SAP by targeting the *Tollip* pathway through miR-128-2-5p.

The ERK/NF- κ B pro-inflammatory pathway is an important inflammatory regulatory pathway.^{51,52} ERK is the most important mediator of cellular transcriptional activities, including inflammatory responses.⁵³ ERK activates the NF- κ B, thereby producing pro-inflammatory compounds (such as TNF- α and IL-6) that aggravate the airway inflammation and destroy the normal alveolar structure.⁵⁴ The effects of PNS 1 on the ERK/NF- κ B pro-inflammatory pathways were also investigated. Results showed that the expression levels of p-ERK1 and NF- κ B increased in the lung tissue, and the lung inflammation in the acute pancreatitis model induced by taurocholate increased too. After the PNS 1 administration, the expression levels of p-ERK1 and NF- κ B decreased in the lung tissue induced by acute pancreatitis. The inflammation in the lung and ALI were reduced. Thus, the *Panax* NG-R1 may play a protective role in the lung by increasing *Tollip* and further blocking the ERK/NF- κ B pro-inflammatory pathway to control the inflammation in the lungs induced by acute pancreatitis.

Previous studies have found that the administration of PNS alleviates the ALI induced by intestinal ischemia/reperfusion⁵⁵ and ameliorates oleic acid- and LPS-induced ALI potentially through the restoration of epithelial sodium channel α mRNA and protein expression.⁵⁶ A 2019 study has shown that NG-R1 up-regulates miR-132 to protect human lung fibroblast MRC-5 cells from the injury caused by LPS.⁵⁷ NG-R1 is suggested to regulate the ALI by regulating the miRNA. This effect is due to the antioxidant and anti-inflammatory effects of PNS. Our research further found that the NG-R1 had the following effects: increased activity of the *Tollip* signaling pathway via the down-regulation of miR-128-2-5p, inhibition of the LR4/MyD88, HMGB1/TLR4/NF- κ B, and ERK/NF- κ B signaling pathways, reduced lung inflammation, and alleviation of the SAP-induced ALI.

Taurocholate-induced pancreatitis animal models have some shortcomings, such as prolonged preparation time, difficult operation, high death rate, and potential infection of the pancreas when puncturing through the gut.⁵⁸ However, compared with clinical trials, the use of animal models have many advantages, such as accessible subjects, standardization of the degree of the lesion, practicability of invasive inspection, adequate tissue samples, and practicability of prophylactic treatment.⁵⁸ Therefore, we chose

taurocholate-induced pancreatitis animal models. *In vivo*, in the process of ALI caused by SAP, the specific lung injury caused by endotoxin and various inflammatory mediators due to pancreatic inflammation can be reflected in the macrophage inflammation model. The endotoxin is involved in the pathogenesis of ALI caused by SAP.⁵⁹ The endotoxin can make mild pancreatitis develop into severe pancreatitis and further cause the occurrence of systemic inflammatory syndrome and ALI.⁵⁹ Thus, we chose LPS-induced macrophage inflammation models.

In recent years, the combination of gas chromatography (GC)–quadrupole time-of-flight mass spectrometry (Q-TOF/MS) and liquid chromatography–Q-TOF/MS has been applied successfully in numerous metabolomics studies to achieve sensitive and accurate metabolic profiling and screening of biomarkers.⁶⁰ In future work, the GC-Q-TOF/MS will be used to analyze the changes in the metabolism of the NG-R1 in different organs in the body and its influence on important metabolic indicators in taurocholate-induced pancreatitis animal models and observe the effects of the NG-R1 on taurocholate-induced pancreatitis animal models.

In China, PNS is clinically used for the treatment of inflammation-related diseases.⁶¹ PNS is usually given intravenously and has a certain therapeutic effect.⁶¹ NG-R1 is one of the main active ingredients of PNS. At present, the use of the NG-R1 alone in clinical treatment has not been reported yet and is still in the stage of animal experimentation, often given orally to treat experimental animals. However, previous studies have shown that NG-R1 is easily dissolved in water but shows remarkably low bioavailability and poor permeability in the gastrointestinal tract.⁶² Therefore, this experiment is chosen to inject NG-R1 intraperitoneally to treat experimental animals.

In conclusion, our experiments illustrated that NG-R1 could extenuate ALI induced by SAP. The mechanism of action may be related to the decreased expression of miR-128-2-5p, increased activity of the *Tollip* signaling pathway, attenuated activity of the HMGB1/TLR4 and ERK1 signaling pathways and inhibited inflammatory response to SAP-induced ALI. *Tollip* was the regulatory target for miR-128-2-5p. Thus, this study provided a new rationale for the use of the NG-R1 in the treatment of inflammatory-related ALI. However, NG-R1 had a complex mechanism of anti-pulmonary injury, which involved inflammation, oxidative stress, and apoptosis-related pathways. The NG-R1 mechanism needs to be further explored. MiR-128-2-5p was involved in the development of ALI induced by SAP, and *Tollip* was the regulatory target for the miR-128-2-5p.

Ethics approval and consent to participate

All experiments were approved by the Ethics Committee of Dali University and performed in accordance with The

Guidelines of the Animal Care Committee of Dali University. The animals were treated humanely consistent with the relevant national, international, and/or institutional guidelines and legislations.

Acknowledgements

The authors are grateful to Enpaper for editing the English text of a draft of this manuscript.

Declaration of conflicting interests

The author(s) declared no potential conflicts of interest with respect to the research, authorship, and/or publication of this article.

Funding

The author(s) disclosed receipt of the following financial support for the research, authorship, and/or publication of this article: This work was supported by the Yunnan Applied Basic Research Project-Union Foundation (grant number 2017FE468[-032]).

Availability of data and materials

All generated or analyzed data in this study are included in this published article.

ORCID iD

Rong-jie Shi  <https://orcid.org/0000-0001-6954-6974>

References

- Pan L, Yu L, Wang L, et al. Inflammatory stimuli promote oxidative stress in pancreatic acinar cells via Toll-like receptor 4/nuclear factor- κ B pathway. *Int J Mol Med* 2018; 42: 3582–3590.
- Zhao Q, Zhang H, Huang J, et al. Melatonin attenuates the inflammatory response via inhibiting the C/EBP homologous protein-mediated pathway in taurocholate-induced acute pancreatitis. *Int J Mol Med* 2018; 42: 3513–3521.
- Wu XM, Ji KQ, Wang HY, et al. microRNA-542–5p protects against acute lung injury in mice with severe acute pancreatitis by suppressing the mitogen-activated protein kinase signaling pathway through the negative regulation of P21-activated kinase 1. *J Cell Biochem* 2019; 20: 290–304.
- Cui HX, Xu JY and Li MQ. Efficacy of continuous renal replacement therapy in the treatment of severe acute pancreatitis associated acute respiratory distress syndrome. *Eur Rev Med Pharmacol Sci* 2014; 18: 2523–2526.
- Shen Y, Wen L, Zhang R, et al. Dihydrodiosgenin protects against experimental acute pancreatitis and associated lung injury through mitochondrial protection and PI3K γ /Akt inhibition. *Br J Pharmacol* 2018; 175: 1621–1636.
- Guo Q, Li P, Wang Z, et al. Brain distribution pharmacokinetics and integrated pharmacokinetics of Panax Notoginsenoside R1, Ginsenosides Rg1, Rb1, Re and Rd in rats after intranasal administration of Panax Notoginseng Saponins assessed by UPLC/MS/MS. *J Chromatogr B Analyt Technol Biomed Life Sci* 2014; 969: 264–271.
- Liu MW, Wei R, Su MX, et al. Effects of Panax notoginseng saponins on severe acute pancreatitis through the regulation of mTOR/Akt and caspase-3 signaling pathway by upregulating miR-181b expression in rats. *BMC Complement Altern Med* 2018; 18: 51.
- Peng XX, Zhang SH, Wang XL, et al. Panax Notoginseng flower saponins (PNFS) inhibit LPS-stimulated NO overproduction and iNOS gene overexpression via the suppression of TLR4-mediated MAPK/NF-kappa B signaling pathways in RAW264.7 macrophages. *Chin Med* 2015; 10: 15.
- Fan JS, Liu DN, Huang G, et al. Panax notoginseng saponins attenuate atherosclerosis via reciprocal regulation of lipid metabolism and inflammation by inducing liver X receptor alpha expression. *J Ethnopharmacol* 2012; 142: 732–738.
- Yan YT, Li SD, Li C, et al. Panax notoginsenoside saponins Rb1 regulates the expressions of Akt/ mTOR/PTEN signals in the hippocampus after focal cerebral ischemia in rats. *Behav Brain Res* 2018; 345: 83–92.
- Yang X, Xiong X, Wang H, et al. Protective effects of panax notoginseng saponins on cardiovascular diseases: a comprehensive overview of experimental studies. *Evid Based Complement Alternat Med* 2014; 2014: 204840.
- Burns K, Clatworthy J, Martin L, et al. Tollip, a new component of the IL-1RI pathway, links IRAK to the IL-1 receptor. *Nat Cell Biol* 2000; 2: 346–351.
- Kim WS, Kim K, Byun EB, et al. RM, a novel resveratrol derivative, attenuates inflammatory responses induced by lipopolysaccharide via selectively increasing the Tollip protein in macrophages: a partial mechanism with therapeutic potential in an inflammatory setting. *Int Immunopharmacol* 2020; 78: 106072.
- Inomata M, Horie T and Into T. Effect of the antimicrobial peptide LL-37 on gene expression of chemokines and 29 Toll-like receptor-associated proteins in human gingival fibroblasts under stimulation with Porphyromonas gingivalis lipopolysaccharide. *Probiotics Antimicrob Proteins* 2020; 12: 64–72.
- Wang X, Liu Y, Wang S, et al. Asparagine reduces the mRNA expression of muscle atrophy markers via regulating protein kinase B (Akt), AMP-activated protein kinase α , toll-like receptor 4 and nucleotide-binding oligomerisation domain protein signalling in weaning piglets after lipopolysaccharide challenge. *Br J Nutr* 2016; 116: 1188–1198.
- Parmar N, Chandrakar P, Vishwakarma P, et al. Leishmania donovani exploits Tollip, a multitasking protein, to impair TLR/IL-1R signaling for its survival in the host. *J Immunol* 2018; 201: 957–970.
- Assmann TS, Recamonde-Mendoza M, de Souza BM, et al. MicroRNAs and diabetic kidney disease: systematic review and bioinformatic analysis. *Mol Cell Endocrinol* 2018; 477: 90–102.
- Xiao M, Li J, Li W, et al. MicroRNAs activate gene transcription epigenetically as an enhancer trigger. *RNA Biol* 2017; 14: 1326–1334.
- van den Berge M and Tasena H. Role of microRNAs and exosomes in asthma. *Curr Opin Pulm Med* 2019; 25: 87–93.
- Dong RF, Zhang B, Tai LW, et al. The neuroprotective role of MiR-124-3p in a 6-hydroxydopamine-induced cell model of parkinson's disease via the regulation of ANAX5. *J Cell Biochem* 2018; 119: 269–277.

21. Wang Y, Zheng F, Gao G, et al. MiR-548a-3p regulates inflammatory response via TLR4/NF- κ B signaling pathway in rheumatoid arthritis. *J Cell Biochem* 2018; 20: 1133–1140.
22. Hussain N, Zhu W, Jiang C, et al. Down-regulation of miR-10a-5p in synoviocytes contributes to TBX5-controlled joint inflammation. *J Cell Mol Med* 2018; 22: 241–250.
23. Kong D and Zhang Z. NAIF1 Suppresses osteosarcoma progression and is regulated by miR-128-2-5p. *Cell Biochem Funct* 2018; 36: 443–449.
24. Geng LJ, Zhang T, Liu W, et al. Inhibition of miR-128-2-5p abates A β -mediated cytotoxicity by targeting PPAR- γ via NF- κ B inactivation in primary mouse cortical neurons and Neuro2a cells. *Yonsei Med J* 2018; 59: 1096–1106.
25. Xia Z, Meng F, Liu Y, et al. Decreased MiR-128-3p alleviates the progression of rheumatoid arthritis by up-regulating the expression of TNFAIP3. *Biosci Rep* 2018; 38: 238–344.
26. Liu MW, Wang YH, Qian CY, et al. Xuebijing exerts protective effects on lung permeability leakage and lung injury by upregulating toll-interacting protein expression in rats with sepsis. *Int J Mol Med* 2014; 34: 1492–1504.
27. Liu S, Gao S, Yang Z, et al. miR-128-3p reduced acute lung injury induced by sepsis via targeting PEL12. *Open Med (Wars)* 2021; 16: 1109–1120.
28. Aho HJ, Koskensalo SM and Nevalainen TJ. Experimental pancreatitis in the rat. Sodium taurocholate-induced acute haemorrhagic pancreatitis. *Scand J Gastroenterol* 1980; 15: 411–416.
29. Papargyri N, Pontoppidan M, Andersen MR, et al. Chemical diversity of locked nucleic acid-modified antisense oligonucleotides allows optimization of pharmaceutical properties. *Mol Ther Nucleic Acids* 2020; 19: 706–717.
30. Fan CL, Qiao Y and Tang MK. Notoginsenoside R1 attenuates high glucose-induced endothelial damage in rat retinal capillary endothelial cells by modulating the intracellular redox state. *Drug Des Devel Ther* 2017; 11: 3343–3354.
31. Zhang J, Ding L, Wang B, et al. Notoginsenoside R1 attenuates experimental inflammatory bowel disease via pregnane X receptor activation. *J Pharmacol Exp Ther* 2015; 352: 315–324.
32. Liu MW, Su MX, Tang DY, et al. Ligustrazin increases lung cell autophagy and ameliorates paraquat-induced pulmonary fibrosis by inhibiting PI3K/Akt/mTOR and hedgehog signaling via increasing miR-193a expression. *BMC Pulm Med* 2019; 19: 35.
33. Zhang J, Zhu Y, Hu L, et al. miR-494 induces EndMT and promotes the development of HCC (hepatocellular carcinoma) by targeting SIRT3/TGF- β /SMAD signaling pathway. *Sci Rep* 2019; 9: 7213.
34. Sun LC, Zhang HB, Gu CD, et al. Protective effect of acacetin on sepsis-induced acute lung injury via its anti-inflammatory and antioxidative activity. *Arch Pharm Res* 2018; 41: 1199–1210.
35. Bi J, Tong L, Zhu X, et al. Keratinocyte growth factor-2 intratracheal instillation significantly attenuates ventilator-induced lung injury in rats. *J Cell Mol Med* 2014; 18: 1226–1235.
36. Szapiel SV, Elson NA, Fulmer JD, et al. Bleomycin-induced interstitial pulmonary disease in the nude, athymic mouse. *Am Rev Respir Dis* 1979; 120: 893–899.
37. Liu MW, Su MX, Zhang W, et al. Protective effect of Xuebijing injection on paraquat-induced pulmonary injury via down-regulating the expression of p38 MAPK in rats. *BMC Complement Altern Med* 2014; 14: 498.
38. Ng QX, Venkatanarayanan N and Ho CY. Clinical use of *Hypericum perforatum* (St John's wort) in depression: a meta-analysis. *J Affect Disord* 2017; 210: 211–221. 37.
39. Shi Z, Ye W, Zhang J, et al. Lipoxin4 attenuates acute pancreatitis-associated acute lung injury by regulating AQP-5 and MMP-9 expression, anti-apoptosis and PKC/SSECKS-mediated F-actin activation. *Mol Immunol* 2018; 103: 78–88.
40. Zhang H, Neuhöfer P, Song L, et al. IL-6 trans-signaling promotes pancreatitis-associated lung injury and lethality. *J Clin Invest* 2013; 123: 1019–1031.
41. Chooklin S. Pathogenic aspects of pulmonary complications in acute pancreatitis patients. *Hepatobiliary Pancreat Dis Int* 2009; 8: 186–192.
42. Wu XM, Ji KQ, Wang HY, et al. MicroRNA-339-3p alleviates inflammation and edema and suppresses pulmonary microvascular endothelial cell apoptosis in mice with severe acute pancreatitis-associated acute lung injury by regulating Anxa3 via the Akt/mTOR signaling pathway. *J Cell Biochem* 2018; 119: 6704–6714.
43. Xiao J, Zhu T, Yin YZ, et al. Notoginsenoside R1, a unique constituent of *Panax notoginseng*, blinds pro-inflammatory monocytes to protect against cardiac hypertrophy in ApoE mice. *Eur J Pharmacol* 2018; 833: 441–450.
44. Zhao L, Li R, Xu S, et al. Tumor suppressor miR-128-2-5p-3p inhibits metastasis and epithelial-mesenchymal transition by targeting ZEB1 in esophageal squamous-cell cancer. *Acta Biochim Biophys Sin (Shanghai)* 2018; 50: 171–180.
45. Jiang J, Feng X, Zhou W, et al. miR-128-2-5p reverses the gefitinib resistance of the lung cancer stem cells by inhibiting the c-met/PI3K/AKT pathway. *Oncotarget* 2016; 7: 73188–73199.
46. Shyamasundar S, Ong C, Yung LL, et al. miR-128-2-5p regulates genes associated with inflammation and fibrosis of Rat kidney cells In vitro. *Anat Rec (Hoboken)* 2018; 301: 913–921.
47. Yan ZZ, Huang YP, Wang X, et al. Integrated omics reveals tollip as a regulator and therapeutic target for hepatic ischemia-reperfusion injury in mice. *Hepatology* 2019; 70: 1750–1769.
48. Saikia P, Roychowdhury S, Bellos D, et al. Hyaluronic acid 35 normalizes TLR4 signaling in Kupffer cells from ethanol-fed rats via regulation of microRNA291b and its target Tollip. *Sci Rep* 2017; 7: 15671.
49. Byun EB, Kim WS, Sung NY, et al. Epigallocatechin-3-gallate regulates anti-inflammatory action through 67-kDa laminin receptor-mediated Tollip signaling induction in lipopolysaccharide-stimulated human intestinal epithelial cells. *Cell Physiol Biochem* 2018; 46: 2072–2081.
50. Fernandes P, MacSharry J, Darby T, et al. Differential expression of key regulators of Toll-like receptors in ulcerative colitis and Crohn's disease: a role for Tollip and peroxisome proliferator-activated receptor gamma? *Clin Exp Immunol* 2016; 183: 358–368.

51. Watts BA, Tamayo E, Sherwood ER, et al. Monophosphoryl lipid A induces protection against LPS in medullary thick ascending limb through induction of Tollip and negative regulation of IRAK-1. *Am J Physiol Renal Physiol* 2019; 317: F705–F719.
52. Romanick SS, Morrill K, Hostler A, et al. HDAC1/2-mediated regulation of JNK and ERK phosphorylation in bovine mammary epithelial cells in response to TNF- α . *J Cell Physiol* 2019; 234: 1088–1098.
53. Li CL, Yan Y, Shi Q, et al. Recuperating lung decoction attenuates inflammation and oxidation in cigarette smoke-induced COPD in rats via activation of ERK and Nrf2 pathways. *Cell Biochem Funct* 2017; 35: 278–286.
54. Sun HJ, Cai WW, Wang X, et al. Vaccaria hypaphorine alleviates lipopolysaccharide-induced inflammation via inactivation of NF- κ B and ERK pathways in Raw 264.7 cells. *BMC Complement Altern Med* 2017; 17: 120.
55. Rong L, Chen Y, He M, et al. Panax notoginseng saponins attenuate acute lung injury induced by intestinal ischaemia/reperfusion in rats. *Respirology* 2009; 14: 890–898.
56. Chen YQ, Rong L and Qiao JO. Anti-inflammatory effects of Panax notoginseng saponins ameliorate acute lung injury induced by oleic acid and lipopolysaccharide in rats. *Mol Med Rep* 2014; 10: 1400–1408.
57. Cong S, Xiang LQ, Yuan XT, et al. Notoginsenoside R1 up-regulates microRNA-132 to protect human lung fibroblast MRC-5 cells from lipopolysaccharide-caused injury. *Int Immunopharmacol* 2019; 68: 137–144.
58. Wittel UA, Wiech T, Chakraborty S, et al. Taurocholate-induced pancreatitis: a model of severe necrotizing pancreatitis in mice. *Pancreas* 2008; 36: e9–21.
59. Li X, Ye C, Mulati M, et al. Ellipticine blocks synergistic effects of IL-17A and TNF-alpha in epithelial cells and alleviates severe acute pancreatitis-associated acute lung injury. *Biochem Pharmacol* 2020; 177: 113992.
60. Wang P, Ng QX, Zhang H, et al. Metabolite changes behind faster growth and less reproduction of daphnia similis exposed to low-dose silver nanoparticles. *Ecotoxicol Environ Saf* 2018; 163: 266–273.
61. Xu Y, Tan HY, Li S, et al. Panax notoginseng for inflammation-related chronic diseases: a review on the modulations of multiple pathways. *Am J Chin Med* 2018; 46: 971–996.
62. Liu H, Yang J, Du F, et al. Absorption and disposition of ginsenosides after oral administration of Panax notoginseng extract to rats. *Drug Metab Dispos* 2009; 37: 2290–2298.